The radical index and the effect of oxygen concentration on non-premixed cool flame extinction of large *n*-alkanes

Mengni Zhou[a,b,*], Omar R. Yehia[a], Wenbin Xu[a], Christopher B. Reuter[a,c], Ziyu Wang[a], Chao Yan[a], Bo Jiang[a], Yiguang Ju[a]

[a]*Department of Mechanical and Aerospace Engineering, Princeton University, NJ 08544, USA*

[b]*School of Energy and Power Engineering, Wuhan University of Technology, Wuhan, Hubei 430063, PR China*

[c]*U.S. Air Force Research Laboratory, Aerospace Systems Directorate, Wright-Patterson AFB, OH 45433, USA*

***Corresponding author**

Mengni Zhou

Department of Mechanical and Aerospace Engineering

Princeton University

Princeton, NJ 08544, USA

Email: mengniz@princeton.edu; zhoumengni@whut.edu.cn

Abstract: The effects of fuel and oxygen concentrations on the extinction limits of non-premixed cool flames for large *n*-alkanes, ranging from *n*-heptane to *n*-dodecane, are measured in an atmospheric counterflow burner. The measurements are used (a) to derive a scaling law between the cool flame reactivity and the oxygen concentration and (b) to develop a radical index to rank the cool flame reactivity of *n*-alkanes, with the assistance of kinetic modeling. First, due to the significant role of multiple oxygen addition reactions in the low-temperature branching sequence, the relationship between cool flame extinction (and hence the chemical time scale) and oxygen concentration are examined. The results suggest that all measured *n*-alkane cool flame extinction limits exhibit similar nonlinear dependence on oxygen concentration. The results further show that, due to the combined effects of multi-oxygen addition processes and the negative temperature coefficient effect, the cool flame low temperature reactivity of *n*-alkanes is proportional to *n*th power of oxygen mole fraction, $[O_2]^n$, with n = 1.5-2. Furthermore, by accounting for thermal and mass transport effects using a mass-weighted enthalpy, a cool flame radical index is proposed to evaluate the role of cool flame reactivity on the extinction limits of large *n*-alkanes. We find that the radical index of large *n*-alkanes increases with the increase of carbon length of the fuel molecules, which is consistent with stronger low-temperature reactivity.
Keywords: Cool flame; cool flame radical index; *n*-alkane; counterflow; extinction limit; oxygen effect; non-premixed flame

1. Introduction

Large *n*-alkanes, which exhibit strong low-temperature reactivity, make up a large proportion of many commercial transportation fuels and their surrogates. For example, *n*-heptane is a primary reference fuel component for gasoline surrogates [1–3]. Furthermore, fuel

components such as *n*-decane [4–6] or *n*-dodecane [7–9] are often used to represent linear paraffins in fuel surrogate formulations. Previous work has shown that the low-temperature reactivity of large *n*-alkanes can establish self-sustaining cool flames [10][11,12] and has important influences on the extension of the lean flammability limit in premixed flames [13–15], mixture ignition [16–18], and engine knock [19,20]. As a result, the low-temperature oxidation of large *n*-alkanes has been studied extensively in various kinetic experiments [10,21–26] in order to develop and validate chemical kinetic models of low-temperature reactivity.

Microgravity *n*-alkane droplet combustion measurements conducted onboard the ISS [27–31], as well as terrestrial counterflow cool flame studies [12,32–34], have provided significant insights into the cool flame chemistry of large *n*-alkanes and their extinction dynamics. The droplet measurements have suggested that the residence times at cool flame extinction for different large *n*-alkane droplets have the same dependence on oxygen concentration [27]. However, counterflow cool flame experiments [32] revealed that the cool flame extinction limits differ significantly depending on the length of the chain. Naturally, one can ask how these two different flame geometries can, at first glance, give different dependences of fuel reactivity on molecule size of *n*-alkanes. Moreover, is it possible to use the counterflow diffusion cool flames to derive a similar oxygen dependence of *n*-alkane fuel reactivity on the oxygen concentration to the results of droplet combustion?

Additionally, although the extinction limits of non-premixed cool flames in the counterflow configuration play a critical role in validating fuel oxidation when coupled with transport and heat release, it is not clear how to delineate the role of kinetics and transport without properly accounting for the variation in the transport properties of the fuel. Specifically, the mass transport influences the distributions of fuel and oxidizer in the flame reaction zone,

which then affect the temperature and reaction rate profiles. Hence, it is important to separate the thermal and mass transport effects for quantifying the effect of chemical kinetics on cool flame extinctions.

The transport-weighted enthalpy and the concept of the radical index were proposed to evaluate the chemical kinetic contributions to non-premixed hot flame extinction [35]. However, the dominant chain-branching reaction pathways in the cool and hot flame are different [10]. The cool flame is governed by the peroxy chemistry related to the large fuel-sized molecules, while chain branching in the hot flame mainly depends on small species oxidation chemistry [10], which leads to differences in their respective flame structure [12,14,36]. In the hot flame of *n*-alkane/air, far from extinction conditions, the fuel is consumed well before the reaction zone, and only negligible oxidizer leaks across the reaction zone. Whereas, in the cool flame, significant leakage of both fuel and oxidizer is observed in the cool flame structure, even far from extinction conditions. Owing to such fundamental differences, it stands to reason that the transport-weighted enthalpy and the radical index proposed for the hot flames in [35] may not be applicable directly to cool flames. Instead, we seek a cool flame radical index that properly accounts for the effects of transport and kinetics. Having such a scaling at hand would simplify the way to screen the low-temperature chemistry of fuels and surrogate fuels. For example, recent measurements have shown the difficulty in tailoring physical and chemical properties of kerosene surrogates to match the target fuel reactivity, even when the DCN of the surrogate matches that of the target [37]. Hence, having a robust screening method for low-temperature reactivity of individual components and blends is therefore crucial for rapid fuel synthesis, particularly since low-temperature ignition characterization in constant volume laboratory-scale can diverge significantly from full-scale engine performance [38].

Motivated by the above, the purpose of this work is to measure the extinction limits of cool flames of large *n*-alkanes and to derive a generic correlation between cool flame reactivity of *n*-alkanes and the oxygen concentration and carbon chain-length. The non-premixed cool flame extinction limits of large *n*-alkanes, ranging from *n*-heptane and *n*-dodecane, at different fuel and oxygen mole fractions are measured in an atmospheric counterflow burner. Using the measured extinction limits, we determine a scaling relationship between the oxygen concentration and the extinction strain rate. In addition, this work examines whether the relationship determined via the counterflow burner is similar to that derived from microgravity droplet combustion experiments [27]. Moreover, to isolate the effects of thermal and mass transport, a mass-weighted cool flame enthalpy and radical index are proposed to scale the impact of low-temperature chemical reactivity on the cool flame extinction limits.

2. Experimental and computational methods

2.1 Experiments

To measure the non-premixed cool flame extinction limits, an atmospheric counterflow is employed. Details of the experimental setup are presented in our previous works [12,36,39]. The experimental counterflow configuration consists of two opposed burners, a liquid fuel injection pump, a liquid fuel atomization and vaporization system, flow controllers, and an ozone generator. A schematic of the experimental setup of the atmospheric counterflow burner is sketched in Fig. 1. The two opposed burners contain a pair of main flow converged nozzles with 13 mm exit diameters maintained at a 22.5 mm separation distance and a pair of co-flow nozzles. Liquid fuel is injected into a heated vaporization chamber using a steel syringe pump (Harvard PHD) and the vaporized fuel gas is carried by pre-heated nitrogen forming a nitrogen-diluted fuel

mixture which ejects through the main nozzle of the upper burner. The oxidizer is ejected from the main flow nozzle of the bottom burner. To isolate the flame from the surrounding environment, nitrogen co-flows are ejected from co-flow nozzles of both upper and bottom burners, maintained at their respective main flow temperatures within 10 K. The measured temperatures of the flow at the nozzle exit center position (the position shown as the red points in Fig. 1) are defined as the burner temperatures. The upper/fuel-side burner temperature (T_f) is maintained at 550 ± 5 K, and the bottom/oxidizer-side burner temperature is maintained at 550 ± 5 K or 300 ± 5 K.

In the present study, *n*-dodecane, *n*-decane, *n*-octane, and *n*-heptane (all Sigma-Aldrich, anhydrous, >99%) are chosen as representative fuels to study low-temperature chemical reactivity in cool flames. To establish non-premixed cool flames of *n*-alkanes/O_2/N_2 mixtures, ozone doping is used to initiate the ozone-assisted cool flame. When the oxidizer-side burner temperature is set at 300 K, O_2 in the oxidizer directly goes through an ozone generator (Ozone Solutions, TG-20) to form ozone. However, the same method does not work well for 550 K cases since ozone would decompose rapidly inside the burner [40]. In that case, ozone is doped directly into the oxidizer stream using a small tube, as shown the blue flow pathway in Fig. 1. After the stable cool flames are established, the ozone generator is turned off and the small ozone supply tube is removed from the oxidizer stream. The cool flame extinction limits are determined by gradually increasing the velocities of the fuel and oxidizer stream (while holding momentum balance) at fixed fuel and oxygen mole fractions until the flame extinguishes. The axial velocity gradient at the oxidizer side is defined as a global strain rate, $a = 2U_o/L[1+(U_f/U_o)(\rho_f/\rho_o)^{1/2}]$, where U_o and U_f are the flow velocities of oxidizer and fuel side streams, ρ_o and ρ_f are the density of the two streams, and L is the separation distance between the burners. The

experimental measurements were repeated at least 3 times and had a maximum scatter of ± 5 s^{-1}, which is within the instrument uncertainty and is appropriate for our purposes.

2.2 Computational and kinetic models

Numerical simulations of cool flame extinction limits were performed using the OPPDIF [41] module of the CHEMKIN package. A similar procedure to the experiments was employed to predict the extinction limits; specifically, the velocities of the fuel and oxidizer streams are simultaneously increased (maintaining momentum balance) at constant fuel and oxygen mole fractions until extinction occurs. A slightly smaller strain rate solution is used as a restart in OPPDIF using the mixture-averaged transport properties. This approach and settings have been validated previously [12,32,42]. Moreover, to determine the heat of low-temperature combustion ($\Delta H_{\text{Low, ig}}$) for evaluating the chemical contribution in cool flame extinction, the homogeneous 0-D reactor module [43] of the CHEMKIN package at constant pressure is used in this work.

Two detailed *n*-alkane models (containing all of the tested *n*-alkanes) from Lawrence Livermore National Laboratory (LLNL model) [44] and RWTH Aachen University (Cai model) [45] were used to model low-temperature oxidation. Based on the conclusions of our previous study [32,34,39] and examination of other recently updated kinetic models in the present study, the CRECK kerosene surrogates model [46] containing both *n*-dodecane and *n*-decane showed greatest fidelity to the measurements and was hence selected for further computations.

3. Results and discussion

The measured and computed non-premixed cool flame extinction strain rates of *n*-dodecane ($nC_{12}H_{26}$), *n*-decane ($nC_{10}H_{22}$), *n*-octane (nC_8H_{18}), and *n*-heptane (nC_7H_{16}) as functions

of fuel and oxygen mole fractions are shown in Fig. 2. To establish cool flames at a lower range of oxygen mole fraction, the initial temperature of the oxidizer-side burner is extended to 550 K. In addition, to examine that the conclusions in this study are not affected by boundary temperature experimental data at the oxidizer temperature of 300 K were also determined. From the experimental results shown in Fig. 2, the extinction strain rates of these *n*-alkane non-premixed cool flames increase with the increase of both fuel and oxygen mole fractions. It also can be noted that, similar to previous findings [32], the extinction strain rates of *n*-alkane with longer chain length are higher than those with shorter ones at the same fuel mole fraction. For example, the extinction limit of the *n*-dodecane cool flame is about a factor of four higher than that of the *n*-octane cool flame at the fuel mole fraction of 0.11 and oxidizer temperature of 550 K. Moreover, as expected, the extinction limits at the temperature of oxidizer-side burner of 550 K are higher than those at 300 K.

To examine the low-temperature reactivity prediction performance of the current kinetic mechanisms, a few of the reduced chemical kinetic models are examined via the present experimental cool flame extinction strain rates, and the comparisons for each fuel are presented in the Fig. S1-S4 of Supplementary Material. Here, only the kinetic model computations with the best agreement with experimental data are shown in Fig. 2. It is found that no single kinetic mechanism shows a reasonable prediction for all tested *n*-alkanes. Specifically, the CRECK lumped kerosene surrogates model [46] shows better predictions for the cool flame extinction limits of *n*-dodecane and *n*-decane, and the reduced Chang model [47] works better for the *n*-octane. However, all of the employed kinetic models over-predict the cool flame extinction strain rates for *n*-heptane by at least a factor of two (and are hence not shown in Fig. 2).

3.1 Effect of oxygen concentration on cool flame extinction

The non-premixed flame extinction limits are governed by the ratio of flow residence time to the chemical reaction time, expressed as the Damköhler number (*Da*). The inverse of extinction strain rate can be regarded as the characteristic flow time in which the heat release of the low-temperature chemistry can barely sustain the cool flame. In the low-temperature chain-branching reaction pathway of cool flame, the reactions of multiple oxygen addition reactions via, $R + O_2 = RO_2$ and $QOOH + O_2 = O_2QOOH$, are two major steps for chain-branching [10] and major exothermic reactions in non-premixed cool flames [39], indicating that the concentration of O_2 will significantly affect the global low-temperature branching rate of cool flames. Moreover, the global low-temperature branching rate (ω) is inversely proportional to low-temperature chemical time scale (τ), which can be approximated as the cool flame residence time at extinction ($1/a_E$).

The measured cool flame residence time at extinction as a function of oxygen molar concentration for *n*-dodecane, *n*-decane, *n*-octane and *n*-heptane, with the corresponding fits, are given in Fig. 3. The margin of error is the standard error of regression slope within the 95% confidence interval. To examine the effect of fuel mole fraction on the slope, experimental data of *n*-dodecane at fuel mole fraction of 0.11 and 0.10 and T_o = 300 K were also measured, and a good agreement in their slopes can be found. Moreover, to extend the range of oxygen concentrations, the temperature of the oxidizer-side was increased to 550 K. Again, a close agreement in slope was observed for *n*-dodecane and *n*-decane at T_o = 300 and 550 K, respectively. These results demonstrate that the oxygen dependence for a specific fuel is weakly affected by the boundary conditions at atmospheric pressure, indicating the slope of oxygen dependence curve represents a fuel property.

Furthermore, as shown in Fig. 3, the slopes of oxygen dependence of the different *n*-alkanes are approximately proportional to $[O]^n$ with $n = 1.7$. To understand the nonlinear oxygen dependence of cool flame extinction, one can simply consider the key forward reactions of R + O_2 = RO_2 (R_1), RO_2 = QOOH (R_2), and QOOH + O_2 = O_2QOOH (R_3) in the low-temperature chain-branching process. We further assume that RO_2 and QOOH are quasi-steady-state species [48]. Hence, it can be deduced that $\omega \sim 1/\tau \sim a_{Ext} \sim [O_2]^2$. Therefore, in this case, the slope of $[O_2]$ and $1/a_E$ in the logarithmic plot is −2. However, in reality, because the reactions occur both forward backwards, the concentration of the O_2 involved in the reactions is strictly lower than the one in $n = 2$, especially for the cool flame near extinction. In addition, the negative temperature coefficient (NTC) effect via these backward reactions and decomposition of QOOH and O_2QOOH further slows down the low temperature reactivity. This explains why the present measured slopes are between −1 and −2. This indicates that the oxygen dependence of the cool flame is different from that of hot flame, in which only one oxygen molecule is involved in the chain-branching process, governed mainly by H + O_2 = OH + O reaction.

On the other hand, as mentioned previously, the relationship between cool flame residence times at extinction and oxygen concentrations for large *n*-alkane was also determined by Nayagam and co-authors [27][29] via microgravity droplet-combustion experiments conducted onboard the ISS with a simplified theoretical model. From their discussion, the logarithmic plot of cool flame residence time at extinction and oxygen concentration should have a slope of around −3/2, based on the assumptions that the low-temperature branching rate through the decomposition of ketohydroperoxides is comparable to the consumption rate of alkyl radicals (R) at near the crossover temperature and that, near extinction, the reaction rates of alkyl

radical unimolecular decomposition and its oxygen addition reaction are equal and also occur at the crossover temperature.

However, these simplified assumptions may not be suitable for the cases in the counterflow configuration. First, the effect of transport property on the extinction limits is not considered in the simplified theoretical model. Moreover, the flame temperature near extinction in the counterflow configuration is not exactly at crossover temperature. Figure 4 gives the calculated flame temperatures near cool flame extinction as a function of the oxygen concentration and the crossover temperatures (approximated by the temperature of the midpoint in NTC region based on ignition delay times) for *n*-dodecane and *n*-decane. Clearly, the flame temperatures near cool flame extinction are far lower than the crossover temperature. At temperatures below the NTC crossover, peroxy branching is more prominent. Hence, the slope would be expected to be closer to $n = 2$. Furthermore, we find that the alkyl radical reaction with oxygen is orders of magnitude faster than alkyl radical decomposition near the extinction of cool flames in the present study, as show in Fig. S5 of Supplementary Material. Based on the relationship of the rates of these two reactions (following the analysis in Ref.[27]), it follows that the slope should indeed be greater than the value of $-3/2$ (a corresponding simple derivation is shown in Supplementary Material). In summary, the previous discussion suggests that a slope of -1.7 is both reasonable and is to be expected.

3.2 A scaling analysis of non-premixed cool flame extinction limits

In the previous section, the measurements suggest that the cool flame extinction limits of *n*-alkanes of different carbon lengths exhibit a similar dependence on oxygen concentration. However, the extinction limits of non-premixed cool flames are governed by the coupling between chemical kinetics, thermal transport, and mass transport. In this section, we develop a

simple scaling that allows for delineating of the contributions of transport and reactivity to cool flame extinction.

Won et al. [35] proposed a transport-weighted enthalpy (TWE) concept to separate the effect of chemical kinetics on the hot flame extinction from the thermal and mass transport term, based on asymptotic analysis [49] and the assumption of flame being very close to the stagnation plane and in the near-equilibrium diffusion flame regime [50]. Moreover, in the TWE scaling, only the fuel diffusion coefficient (which scales as the inverse of the square root of the fuel molecular weight) was employed to evaluate the transport property. This is not appropriate for cases in which the flames are located on the fuel side of the stagnation plane [32], as shown the failed rescaling of the hot flame extinction limits for counterflow *n*-alkane/N_2 vs O_2 mixtures by TWE and by the flame structure of one representative *n*-alkane (*n*-decane) near flame extinction in Figs. S6 and S7 of Supplementary Material, respectively. Since the fuel can be simply convected by the bulk flow, therefore, the diffusivity of the reactants should be based on the diffusion coefficient of oxygen. This suggests that the original TWE would over-emphasize the influence of fuel diffusivity for the cases with the flame on the fuel side of the stagnation plane.

For all cases presented, the cool flame is situated on the fuel side of the stagnation plane. Moreover, due to the fact that the low-temperature kinetic process is relatively slow, significant leakage of both fuel and oxidizer is observed in the cool flame structure [31]. Therefore, we posit that the same idea of TWE scaling cannot be directly applied to predict the cool flame extinction limits. Considering the large leakage of fuel across the cool flame, the transport property for cool flame can be simply regarded as the rate of transport by convection. Under the same velocity of the bulk flow, the mass flux depends on the density of the advected material. For simplicity, the

contribution of transport in cool flame extinction may be normalized as the density of the fuel (ρ_{fuel}) and nondimensionalized by the density of nitrogen (ρ_{fuel}/ρ_{n2}).

As for the thermal effect, the heat release of low-temperature combustion of different *n*-alkanes needs to be appropriately accounted for. The heat release of low-temperature oxidation can be approximated as the enthalpy change of the low-temperature ignition stage ($\Delta H_{Low,ig}$) of a *n*-alkane/O_2 mixture at stoichiometric conditions. Since the fuel is partially oxidized to intermediate species in the low-temperature ignition process (or cool flame), it is difficult to infer the enthalpy change for this non-equilibrium process. Based on the temperature profile, $\Delta H_{Low,ig}$ is defined as the difference between the corresponding formation and sensible enthalpy of the mixtures at the initial state and at the point of the minimum local dT/dt gradient during the period after low-temperature ignition and before high-temperature ignition, as shown in Fig. 5.

Since the low-temperature heat release is contributed to by many reactions of different intermediate species, the reduction of a detailed mechanism would cause large deviations in the predicted heat release [32]. Two detailed mechanisms containing all tested *n*-alkanes, Lawrence Livermore National Laboratory (LLNL model) [44] and RWTH Aachen University (Cai model) [45], are used in the present homogeneous ignition simulations. The calculated heat release of low-temperature combustion from the ignition simulations at the experimental temperature of 550 K and atmospheric pressure are summarized in Table 1.

From the discussion above, the thermal and transport effects on the cool flame extinction limit might be scaled by the product of fuel concentration, [Fuel], oxygen concentration, [O_2], the ratio of fuel to nitrogen density, ρ_{fuel}/ρ_{n2}, and the heat release of low-temperature combustion, $\Delta H_{Low,ig}$. For simplicity, the [Fuel] × [O_2] × ΔH_{Low_ig} × ρ_{fuel}/ρ_{n2} produced is termed the mass-weighted enthalpy.

Table 1. The employed enthalpy of low-temperature combustion and density for *n*-dodecane, *n*-decane, *n*-octane and *n*-heptane.

Fuel	ρ [kg/m^3]	$\Delta H_{\mathrm{Low,ig,LLNL}}$ [kcal/mol]	$\Delta H_{\mathrm{Low,ig,Cai}}$ [kcal/mol]
$n\mathrm{C_{12}H_{26}}$	3.954	32.37	30.25
$n\mathrm{C_{10}H_{22}}$	3.241	26.48	25.29
$n\mathrm{C_8H_{18}}$	2.572	20.65	19.95
$n\mathrm{C_7H_{16}}$	2.248	17.81	16.44

3.3 Chemical kinetic contribution at a constant mass-weighted enthalpy

To discern the validity of the mass-weighted enthalpy as a parameter to account for the contributions of thermal and mass transport in cool flame extinction, numerical simulations are examined at first. From the previous validation of kinetic models, the lumped kerosene model from CRECK modeling group [46] can reasonably predict the cool flame extinction limit for both *n*-dodecane and *n*-decane, and the Chang model shows a better performance for *n*-octane. However, the calculated heat release of low-temperature combustion from Chang model for *n*-octane is much lower than that predicted by the detailed LLNL and Cai models, while the lumped kerosene model gives closer values to the detailed models for *n*-dodecane and *n*-decane (see Table S1 in the Supplementary Material). Hence, numerical computations of *n*-dodecane/N_2-O_2 (X_f = 0.100) and *n*-decane/N_2-O_2 (X_f = 0.145) non-premixed cool flames at a fixed value of mass-weighted enthalpy ($\Delta H_{\mathrm{Low,ig}}$ evaluated by CRECK model) are discussed.

The maximum temperature represents the reactivity of the cool flame and strongly depends on the heat of the low-temperature oxidation of the fuel. In addition, the heat release rate is governed by the amount of fuel transported into the reaction zone and burned. Hence, these two properties were examined to evaluate the enthalpy flux into the reaction zone. Figure 6 gives the calculated maximum flame temperature and heat release rate as functions of Damköhler

number, defined as a_E/a, at oxidizer-side temperatures of 550 and 300 K. The maximum flame temperatures and heat release rates collapse for the different fuels at fixed mass-weighted enthalpy. This supports the appropriateness of mass-weighted enthalpy parameter to characterize the enthalpy flux into the reaction zone, demonstrating that the thermal and mass transport effects on non-premixed cool flame extinction limits can be successfully scaled by the mass-weighted enthalpy.

The results in Fig. 6 shows that the contributions of thermal and mass transport on the cool flame extinction limits can be normalized by the mass-weighted enthalpy. The measured cool flame extinction strain rates for *n*-alkanes as a function of the mass-weighted enthalpy (the calculated $\Delta H_{\mathrm{Low,ig}}$ from LLNL model) are shown in Fig. 7. Note that the cool flame extinction strain rate of all measured *n*-alkanes from Fig. 2 are rescaled into two groups, depending on the oxidizer-side temperature, by the mass-weighted enthalpy metric. For the cases at the same initial oxidizer-side temperature, it is seen that the extinction strain rate of *n*-decane is slightly lower than the one of *n*-dodecane. Further, the extinction strain rates of these *n*-alkanes are gradually smaller with the decrease of carbon number after normalizing by the mass-weighted enthalpy, demonstrating that the low-temperature chemical kinetics of the cool flame extinction limits for these *n*-alkanes becomes weaker with the decrease of the chain length.

The hydroxyl (OH) radical plays a dominant role in fuel consumption and heat production in the non-premixed cool flame [10]. In this work, the maximum OH concentration and OH profile thickness as functions of Damköhler number for *n*-dodecane and *n*-decane at a constant mass-weighted enthalpy are used to examine the difference of the chemical kinetic contribution, as shown in Fig. 8. The OH profile thickness is defined as 99.7% of the full width of the OH profile determined by fitting Gaussian distribution. With the decrease of Damköhler

number, the OH profile thickness becomes thinner due to the chemical reaction time becoming shorter relative to the increasing flow time scale causing weaker fuel oxidation. Further, the OH profile thickness at different oxidizer-side temperatures remains almost the same at fixed Damköhler number for different fuels, even though the flame temperatures are different (seen in Fig. 6), indicating the OH distribution in the flame is insensitive to the boundary temperature at a fixed ratio of chemical and flow time scale. Since the non-premixed flames are sensitive to the fuel and oxygen concentration, the concentration of reactants would have a significant impact on the OH profile thickness. Further discussion on the effects of fuel and oxygen concentration on the flame thickness are provided in the Fig. S8 of Supplementary Material. We find that the OH profile thickness decreases with the increase of the fuel and oxygen concentration at the constant Damköhler number.

It is also shown in Fig.8 that the maximum concentration of OH radicals is sensitive to the boundary temperatures. The maximum concentration of OH radicals at oxidizer temperature of 550 K is higher than the one at 300 K, due to higher heat loss in the latter case. Moreover, the peak OH concentration increases with the decreasing Damköhler number, although the flame temperature continually decreases. This is caused by the branching reactions (generating multiple OH radicals) being favored more than chain-propagating reactions at low temperatures (NTC kinetics). Note that OH concentration decreases with the decreasing Damköhler number in hot diffusion flame due to the chain-branching reactions (i.e. $H + O_2 = O + OH$) are faster at higher temperature in hot flames [35]. Further, a small difference in OH concentrations for *n*-dodecane and *n*-decane is observed, indicating a slight difference in their low-temperature chemical kinetic contribution to the cool flame extinction limits.

As shown in Fig. 7, the effects of low-temperature chemical kinetics on the cool flame extinction of the tested alkanes are different. Accordingly, the contribution of their respective low-temperature reactivities needs to be quantified. In our previous study [35], a radical index concept (basing on the OH formation rate) was proposed to represent the kinetic contribution to the flame extinction limits. However, as mentioned previously, none of the current kinetic models can reasonably predict the cool flame extinction limits of the tested fuels. Moreover, the measurement of OH radical concentrations in cool flames is not easily accessible in the current configuration using traditional optical diagnostics (e.g., OH laser-induced fluorescence) due to the very low signal-to-noise ratio (as the OH concentration is several orders of magnitude lower than that present in hot flames at atmospheric conditions). Hence, currently, it is not possible to determine measure the radical index based on the OH radical to quantify the kinetic contribution for all tested *n*-alkanes.

Instead, the chemical kinetic contribution (represented by RI) of each *n*-alkane can be directly inferred by collapsing the extinction strain rates onto a single curve. In this work, *n*-dodecane is set as a reference fuel with a unity cool flame radical index (RI = 1). With RI = 1 defined for *n*-dodecane cool flames, the chemical kinetic contributions of *n*-decane, *n*-octane, *n*-heptane relative to *n*-dodecane are determined accordingly and shown in Fig. 9. By using the cool flame RI and the mass-weighted enthalpy, the low-temperature reactivity of *n*-alkanes can be discerned and ranked. With the decreasing of the chain length, the low-temperature reactivity decreases. To examine the influence of the detailed kinetic model for evaluating $\Delta H_{\mathrm{Low,ig}}$ in rescaling the experimental data, the one using the calculated $\Delta H_{\mathrm{Low,ig}}$ from the other detailed *n*-alkanes models (Cai model) is compared and shown in Fig. S9 and S10 of Supplementary Material. We find that the effect of the calculated $\Delta H_{\mathrm{Low,ig}}$ using these two different detailed

kinetic models on the determination of chemical kinetic contribution is negligible. Therefore, using the measurements of counterflow cool flame extinction limits, one can rank the fuel low temperature reactivity quantitatively and conveniently by using the cool flame radical index, which can rapidly accelerate surrogate component formulation and fuel screening, especially for oxygenated fuels which may have different low temperature reactivities and dependence on oxygen concentration [51].

4. Conclusion

The extinction limits of non-premixed cool flames of large *n*-alkanes ranging from *n*-heptane to *n*-dodecane measured in an atmospheric counterflow burner. The results demonstrate that an increase in fuel and oxygen concentration increases the cool flame extinction limit. In addition, with the increase in the carbon chain length of the *n*-alkane, the cool extinction limit also increases. The results also demonstrate that the dependence of cool flame extinction limit on ambient oxygen concentration for different *n*-alkanes is similar. The results are consistent with the measurements of extinction conditions in microgravity *n*-alkane-droplet experiments [27,29]. The results also demonstrate that, due to the combined effects of multi-oxygen addition processes and the negative temperature coefficient effect, the cool flame low-temperature reactivity of *n*-alkanes is proportional to *n*th power of oxygen mole fraction, $[O_2]^n$. In this study, we measured $n = 1.7$, which is greater than $n = 1.5$ derived from the microgravity droplet experiment. The increase is due to the estimated NTC crossover temperature and radical dissociation being higher than the peak cool flame temperature predicted with detailed chemistry and transport effects.

Furthermore, we also found that the transport-weighted enthalpy and radical index proposed for non-premixed hot flames are not directly applicable to the cool flames because of the existence of fuel and oxygen leakage in cool flames and the location of the flame with respect to the stagnation plane. By accounting for the cool flame thermal and mass transport effects with a mass-weighted enthalpy, a cool flame radical index was proposed to evaluate the cool flame reactivity and to correlate the extinction limits of large *n*-alkanes with different carbon lengths. The results showed that the cool flame extinction limits of *n*-alkanes collapse for the combination of the cool flame radical index and the mass-weighted enthalpy. In addition, the results showed that, with the increase of the chain length of the fuel molecule, the cool flame radical index increases. The derived scaling relation and radical index provide an alternative and convenient metric to evaluate low-temperature reactivity for new fuels and surrogate fuel mixtures. Further work to extend the current results to fuels with different moieties (and hence radical indices) is warranted and is of practical relevance.

Acknowledgment

The authors acknowledge financial support from NASA microgravity grant NNX16AK07G, ARO grant W911NF-16-1-0076, and DOE BES research grant DE-SC0021135.

References

[1] F.L. Dryer, Chemical kinetic and combustion characteristics of transportation fuels, Proc. Combust. Inst. 35 (2015) 117–144.

[2] M. Mehl, W.J. Pitz, C.K. Westbrook, H.J. Curran, Kinetic modeling of gasoline surrogate components and mixtures under engine conditions, Proc. Combust. Inst. 33 (2011) 193–200.

[3] G. Li, M. Zhou, Z. Zhang, J. Liang, H. Ding, Experimental and kinetic studies of the effect of CO2 dilution on laminar premixed n-heptane/air flames, Fuel. 227 (2018) 355–366.

[4] S. Honnet, K. Seshadri, U. Niemann, N. Peters, A surrogate fuel for kerosene, Proc. Combust. Inst. 32 I (2009) 485–492.

[5] S. Dooley, S.H. Won, M. Chaos, J. Heyne, Y. Ju, F.L. Dryer, K. Kumar, C.J. Sung, H. Wang, M.A. Oehlschlaeger, R.J. Santoro, T.A. Litzinger, A jet fuel surrogate formulated by real fuel properties, Combust. Flame. 157 (2010) 2333–2339.

[6] Z. Wang, N. Hansen, A.W. Jasper, B. Chen, D.M. Popolan-Vaida, K.K. Yalamanchi, A. Najjar, P. Dagaut, S.M. Sarathy, Cool flame chemistry of diesel surrogate compounds: n-Decane, 2-methylnonane, 2,7-dimethyloctane, and n-butylcyclohexane, Combust. Flame. 219 (2020) 384–392.

[7] S. Dooley, S.H. Won, J. Heyne, T.I. Farouk, Y. Ju, F.L. Dryer, K. Kumar, X. Hui, C.J. Sung, H. Wang, M.A. Oehlschlaeger, V. Iyer, S. Iyer, T.A. Litzinger, R.J. Santoro, T. Malewicki, K. Brezinsky, The experimental evaluation of a methodology for surrogate fuel formulation to emulate gas phase combustion kinetic phenomena, Combust. Flame. 159 (2012) 1444–1466.

[8] D. Kim, J. Martz, A. Violi, A surrogate for emulating the physical and chemical properties of conventional jet fuel, Combust. Flame. 161 (2014) 1489–1498.

[9] Y.X. Liu, S. Richter, C. Naumann, M. Braun-Unkhoff, Z.Y. Tian, Combustion study of a surrogate jet fuel, Combust. Flame. 202 (2019) 252–261.

[10] Y. Ju, C.B. Reuter, O.R. Yehia, T.I. Farouk, S.H. Won, Dynamics of cool flames, Prog. Energy Combust. Sci. (2019) 100787.

[11] C.H. Sohn, H.S. Han, C.B. Reuter, Y. Ju, S.H. Won, Thermo-kinetic dynamics of near-limit cool diffusion flames, Proc. Combust. Inst. 36 (2017) 1329–1337.

[12] O.R. Yehia, C.B. Reuter, Y. Ju, Kinetic effects of n-propylbenzene on n-dodecane counterflow nonpremixed cool flames, Combust. Flame. 208 (2019) 262–272.

[13] Y. Ju, C.B. Reuter, S.H. Won, Numerical simulations of premixed cool flames of dimethyl ether/oxygen mixtures, Combust. Flame. 162 (2015) 3580–3588.

[14] E. Lin, C.B. Reuter, Y. Ju, Dynamics and burning limits of near-limit hot, warm, and cool diffusion flames of dimethyl ether at elevated pressures, Proc. Combust. Inst. 37 (2019) 1791–1798.

[15] W. Liang, C.K. Law, Extended flammability limits of n-heptane/air mixtures with cool flames, Combust. Flame. 185 (2017) 75–81.

[16] S. Tanaka, F. Ayala, J.C. Keck, J.B. Heywood, Two-stage ignition in HCCI combustion and HCCI control by fuels and additives, Combust. Flame. 132 (2003) 219–239.

[17] Y. Yang, J.E. Dec, N. Dronniou, M. Sjöberg, Tailoring HCCI heat-release rates with partial fuel stratification: Comparison of two-stage and single-stage-ignition fuels, Proc. Combust. Inst. 33 (2011) 3047–3055.

[18] P. Zhao, C.K. Law, The role of global and detailed kinetics in the first-stage ignition delay in NTC-affected phenomena, Combust. Flame. 160 (2013) 2352–2358.

[19] P.R. Ballinger, P.R. Ryason, Isolated stable cool flames of hydrocarbons, Symp. Combust. 13 (1971) 271–277.

[20] Z. Wang, H. Liu, R.D. Reitz, Knocking combustion in spark-ignition engines, Prog. Energy Combust. Sci. 61 (2017) 78–112.

[21] D.F. Davidson, S.C. Ranganath, K.Y. Lam, M. Liaw, Z. Hong, R.K. Hanson, Ignition delay time measurements of normal alkanes and simple oxygenates, J. Propuls. Power. 26 (2010) 280–287.

[22] H.P.S. Shen, J. Steinberg, J. Vanderover, M.A. Oehlschlaeger, A Shock tube study of the ignition of n-heptane, n-decane, n-dodecane, and n-tetradecane at elevated pressures, Energy and Fuels. 23 (2009) 2482–2489.

[23] J.F. Griffiths, P.A. Halford-Maw, D.J. Rose, Fundamental features of hydrocarbon autoignition in a rapid compression machine, Combust. Flame. 95 (1993) 291–306.

[24] S. Jahangirian, S. Dooley, F.M. Haas, F.L. Dryer, A detailed experimental and kinetic modeling study of n-decane oxidation at elevated pressures, Combust. Flame. 159 (2012) 30–43.

[25] H. Zhong, X. Mao, A.C. Rousso, C.L. Patrick, C. Yan, W. Xu, Q. Chen, G. Wysocki, Y. Ju, Kinetic study of plasma-assisted n-dodecane/O2/N2 pyrolysis and oxidation in a nanosecond-pulsed discharge, Proc. Combust. Inst. (2020), https://doi.org/10.1016/j.proci.2020.06.016.

[26] P. Grajetzki, T. Onda, H. Nakamura, T. Tezuka, K. Maruta, Investigation of the chemical and dilution effects of major EGR constituents on the reactivity of PRF by weak flames in a micro flow reactor with a controlled temperature profile, Combust. Flame. 209 (2019) 13–26.

[27] V. Nayagam, D.L. Dietrich, M.C. Hicks, F.A. Williams, Cool-flame extinction during n-alkane droplet combustion in microgravity, Combust. Flame. 162 (2015) 2140-2147.

[28] V. Nayagam, D.L. Dietrich, P. V. Ferkul, M.C. Hicks, F.A. Williams, Can cool flames support quasi-steady alkane droplet burning?, Combust. Flame. 159 (2012) 3583–3588.

[29] F.A. Williams, V. Nayagam, Cool-flame dodecane-droplet extinction diameters, Combust. Flame. 212 (2020) 242–244.

[30] T.I. Farouk, D. Dietrich, F.E. Alam, F.L. Dryer, Isolated n-decane droplet combustion - Dual stage and single stage transition to "Cool Flame" droplet burning, Proc. Combust. Inst. 36 (2017) 2523–2530.

[31] F.A. Williams, V. Nayagam, Quasi-steady combustion of normal-alkane droplets supported by Cool-Flame chemistry near diffusive extinction, Combust. Theory Model. 23 (2019) 748–770.

[32] C.B. Reuter, M. Lee, S.H. Won, Y. Ju, Study of the low-temperature reactivity of large n-alkanes through cool diffusion flame extinction, Combust. Flame. 179 (2017) 23–32.

[33] C.B. Reuter, S.H. Won, Y. Ju, Experimental study of the dynamics and structure of self-sustaining premixed cool flames using a counterflow burner, Combust. Flame. 166 (2016) 125–132.

[34] M. Zhou, O.R. Yehia, C.B. Reuter, C.M. Burger, Y. Murakami, H. Zhao, Y. Ju, Kinetic effects of NO addition on n-dodecane cool and warm diffusion flames, Proc. Combust. Inst. (2020), https://doi.org/10.1016/j.proci.2020.06.002.

[35] S.H. Won, S. Dooley, F.L. Dryer, Y. Ju, A radical index for the determination of the chemical kinetic contribution to diffusion flame extinction of large hydrocarbon fuels, Combust. Flame. 159 (2012) 541–551.

[36] S.H. Won, W. Sun, Y. Ju, Kinetic effects of toluene blending on the extinction limit of n-decane diffusion flames, Combust. Flame. 157 (2010) 411–420.

[37] S. Alkhayat, M. Trivedi, N. Henein, S. Mukhopadhyay, P. Schihl, Experimental validation of a three-component surrogate for Sasol-Isoparaffinic Kerosene in single cylinder diesel engine and ignition quality tester, J. Eng. Gas Turbines Power. 140 (2018).

[38] S.A. Alkhayat, G.D. Joshi, N. Henein, Analysis and Correlation of Ignition Delay for Hydrotreated Vegetable Oil and Ultra Low Sulfur Diesel and Their Blends in Ignition Quality Tester, Fuel. 289 (2021) 119816.

[39] O.R. Yehia, C.B. Reuter, Y. Ju, On the chemical characteristics and dynamics of n-alkane low-temperature multistage diffusion flames, Proc. Combust. Inst. 37 (2019) 1717–1724.

[40] T. Ombrello, S.H. Won, Y. Ju, S. Williams, Flame propagation enhancement by plasma excitation of oxygen. Part I: Effects of O3, Combust. Flame. 157 (2010) 1906–1915.

[41] A.E. Lutz, R.J. Kee, J.F. Grcar, F.M. Rupley, OPPDIF: A FORTRAN program for computing opposed-flow diffusion flames, Report No. SAND-96-8243, Sandia National Laboratories, Livermore, CA, USA, 1997.

[42] C.B. Reuter, R. Zhang, O.R. Yehia, Y. Rezgui, Y. Ju, Counterflow flame experiments and chemical kinetic modeling of dimethyl ether/methane mixtures, Combust. Flame. 196 (2018) 1–10.

[43] A.E. Lutz, R.J. Kee, J.A. Miller, A FORTRAN program for predicting homogeneous gas phase chemical kinetics with sensitivity analysis, Report No. SAND-87-8248, Sandia National Laboratories, Livermore, CA, USA,1997.

[44] S.M. Sarathy, C.K. Westbrook, M. Mehl, W.J. Pitz, C. Togbe, P. Dagaut, H. Wang, M.A. Oehlschlaeger, U. Niemann, K. Seshadri, P.S. Veloo, C. Ji, F.N. Egolfopoulos, T. Lu,

Comprehensive chemical kinetic modeling of the oxidation of 2-methylalkanes from C7 to C20, Combust. Flame. 158 (2011) 2338–2357.

[45] L. Cai, H. Pitsch, S.Y. Mohamed, V. Raman, J. Bugler, H. Curran, S.M. Sarathy, Optimized reaction mechanism rate rules for ignition of normal alkanes, Combust. Flame. 173 (2016) 468–482.

[46] E. Ranzi, A. Frassoldati, A. Stagni, M. Pelucchi, A. Cuoci, T. Faravelli, Reduced kinetic schemes of complex reaction systems: Fossil and biomass-derived transportation fuels, Int. J. Chem. Kinet. 46 (2014) 512–542.

[47] Y. Chang, M. Jia, Y. Liu, Y. Li, M. Xie, H. Yin, Application of a decoupling methodology for development of skeletal oxidation mechanisms for heavy n-alkanes from n-octane to n-hexadecane, Energy and Fuels. 27 (2013) 3467–3479.

[48] N. Kurimoto, B. Brumfield, X. Yang, T. Wada, P. Diévart, G. Wysocki, Y. Ju, Quantitative measurements of HO2/H2O2 and intermediate species in low and intermediate temperature oxidation of dimethyl ether, Proc. Combust. Inst. 35 (2015) 457–464.

[49] F. Liu, G.J. Smallwood, Ö.L. Gülder, Y. Ju, Asymptotic analysis of radiative extinction in counterflow diffusion flames of nonunity Lewis numbers, Combust. Flame. 121 (2000) 275–287.

[50] A. Linan, A. Crespo, An Asymptotic Analysis of Unsteady Diffusion Flames for Large Activation Energies, Combust. Sci. Technol. 14 (1976) 95–117.

[51] B. Rotavera, Influence of Functional Groups on Low-Temperature Combustion Chemistry of Biofuels, Combust. Webinar. (03/06/2021), https://youtu.be/uCLHoE87PZ4.

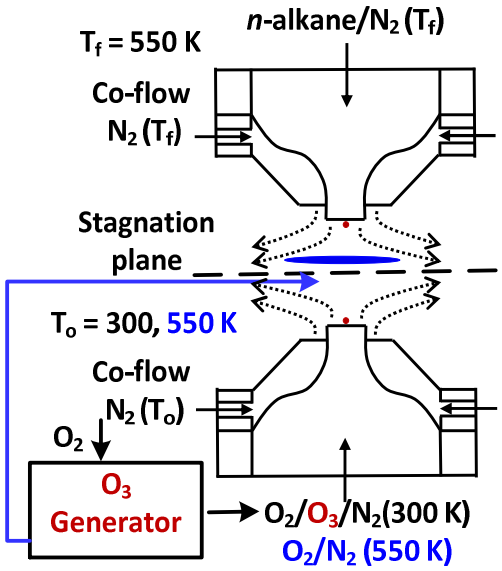

Fig.1. Schematic of experimental setup of the atmospheric counterflow burner.

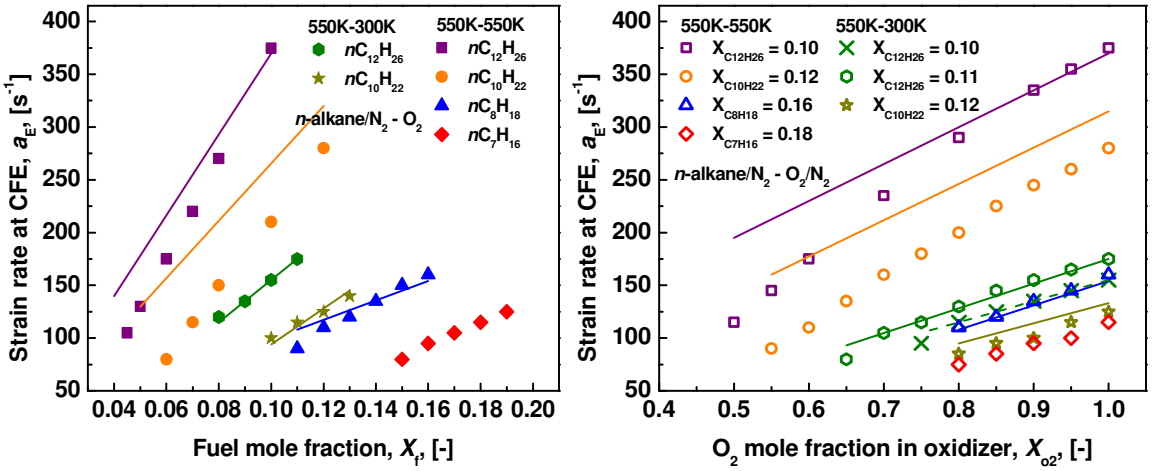

Fig. 2. Measured and predicted cool flame extinction strain rates as functions of fuel (left) or oxygen (right) mole fraction for *n*-dodecane, *n*-decane, *n*-octane, and *n*-heptane flames. Kinetic models for *n*-dodecane and *n*-decane from [46] and for *n*-octane from [47].

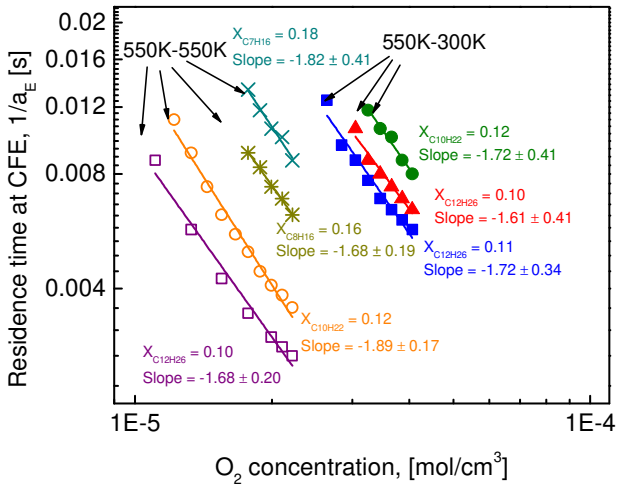

Fig. 3. Cool flame residence time at extinction as a function of oxygen molar concentration for large *n*-alkane diffusion flames at initial oxidizer temperature of 550 and 300 K.

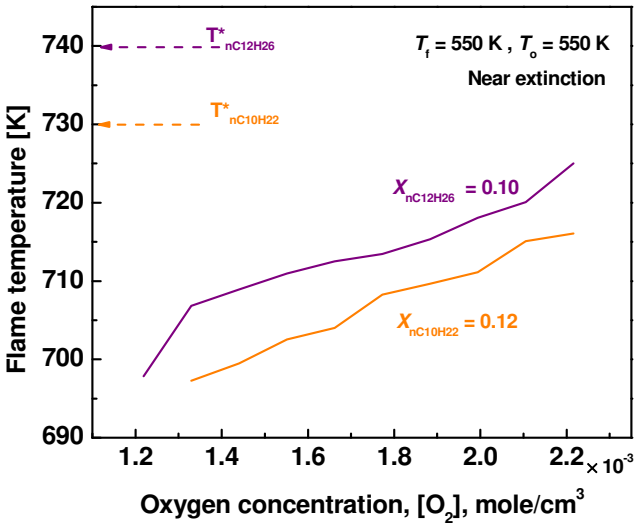

Fig. 4. Calculated flame temperatures near cool flame extinction as a function of oxygen concentration for *n*-dodecane and *n*-decane (kinetic model from [46]). Calculated crossover temperatures are also indicated at the top left.

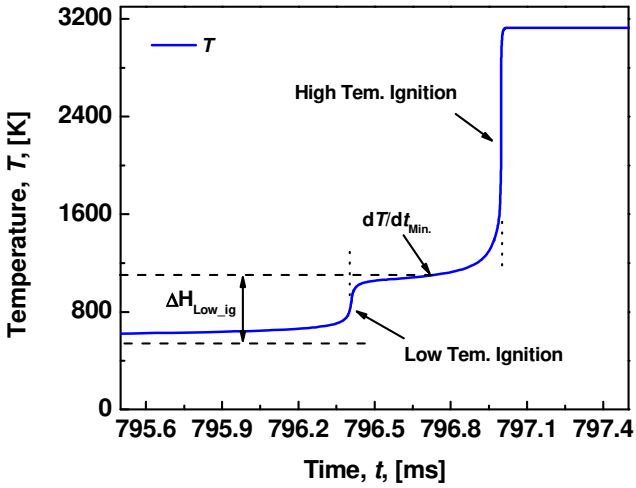

Fig. 5. Calculated temperature profiles versus time history in ignition of *n*-dodecane/O_2 at equivalence ratio of 1.0 and initial temperature of 550 K (Kinetic model from [44]).

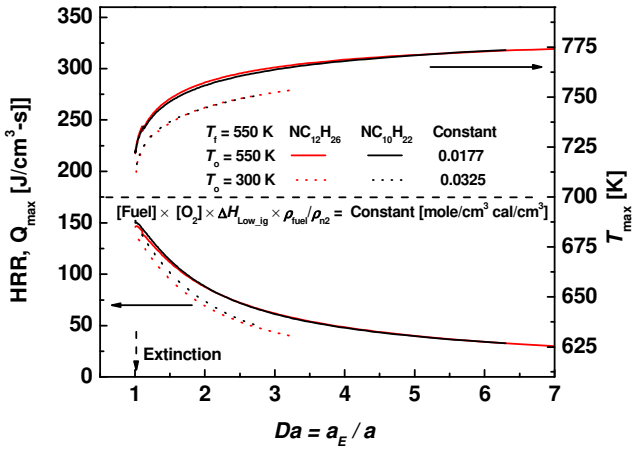

Fig. 6. Computational results of maximum flame temperatures and heat release rates versus Damköhler number for *n*-dodecane and *n*-decane with a constant mass-weighted enthalpy (shown in the figure) at oxidizer-side temperature of 550 and 300 K.

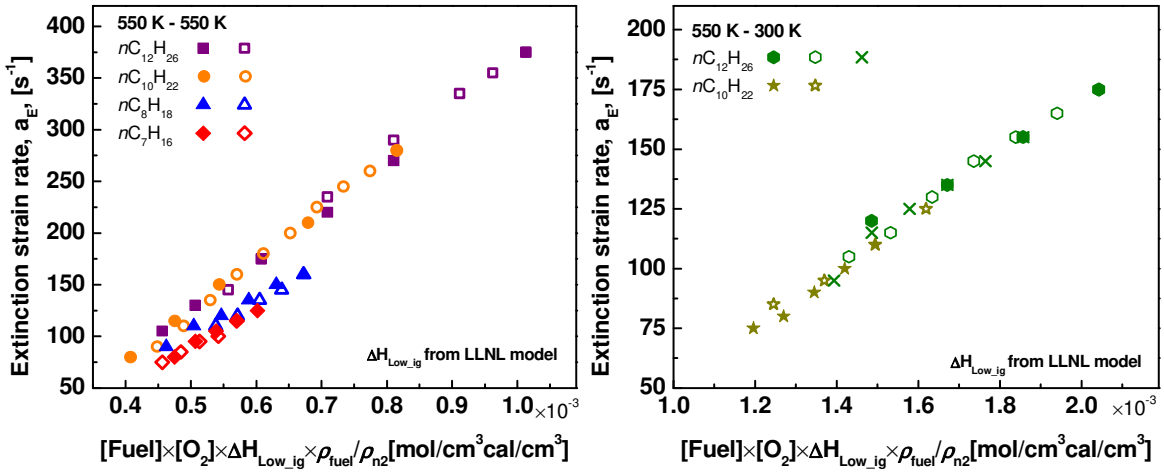

Fig. 7. Cool flame extinction strain rates as a function of mass-weighted enthalpy for *n*-dodecane, *n*-decane, *n*-octane, and *n*-heptane at oxidizer-side temperature of 550 and 300 K.

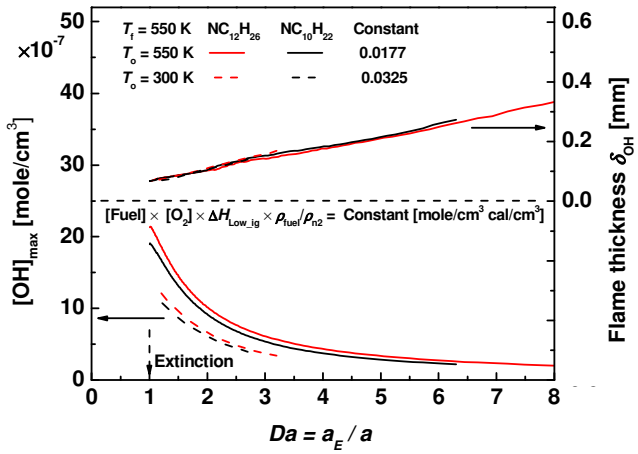

Fig. 8. Computational results of flame thickness and maximum OH concentration versus Damköhler number for *n*-dodecane and *n*-decane with a constant mass-weighted enthalpy (shown in the figure) at oxidizer-side temperature of 550 and 300 K.

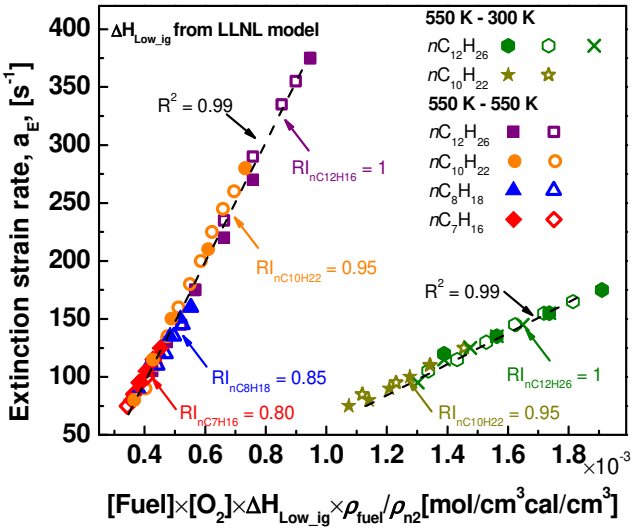

Fig. 9. Rescaled cool flame extinction strain rate of all tested fuels in terms of RI × [Fuel] × [O_2] × $\Delta H_{Low\_ig} \times \rho_{fuel} / \rho_{n2}$; Line: linear fit of all experimental measurements.